



# UNIVERSITÀ DI PARMA

## ARCHIVIO DELLA RICERCA

University of Parma Research Repository

In Search of the Ultimate Benzene Sensor: The EtQxBox Solution

This is the peer reviewed version of the following article:

*Original*

In Search of the Ultimate Benzene Sensor: The EtQxBox Solution / Trzcinski, Jakub W.; Pinalli, Roberta; Riboni, Nicolo'; Pedrini, Alessandro; Bianchi, Federica; Zampolli, Stefano; Elmi, Ivan; Massera, Chiara; Ugozzoli, Franco; Dalcanale, Enrico. - In: ACS SENSORS. - ISSN 2379-3694. - 4:2(2017), pp. 590-598. [10.1021/acssensors.7b00110]

*Availability:*

This version is available at: 11381/2826884 since: 2021-09-29T16:12:19Z

*Publisher:*

American Chemical Society

*Published*

DOI:10.1021/acssensors.7b00110

*Terms of use:*

Anyone can freely access the full text of works made available as "Open Access". Works made available

*Publisher copyright*

note finali coverpage

(Article begins on next page)

02 May 2026

# In Search of the Ultimate Benzene Sensor: The EtQxBox Solution

Jakub Trzciński,<sup>†,‡,§</sup> Roberta Pinalli,<sup>†</sup> Nicolò Riboni,<sup>†</sup> Alessandro Pedrini,<sup>†</sup> Federica Bianchi,<sup>†,‡,§</sup> Stefano Zampolli,<sup>§</sup> Ivan Elmi,<sup>§</sup> Chiara Massera,<sup>†</sup> Franco Uguzzoli,<sup>||</sup> and Enrico Dalcanale<sup>\*,†</sup>

<sup>†</sup>Dipartimento di Scienze Chimiche, della Vita e della Sostenibilità Ambientale, Università di Parma and INSTM UdR Parma, Parco Area delle Scienze 17/A, 43124 Parma, Italy

<sup>‡</sup>Centro Interdipartimentale per l'Energia e l'Ambiente, Università di Parma, Parco Area delle Scienze, Podere Campagna, 43124 Parma, Italy

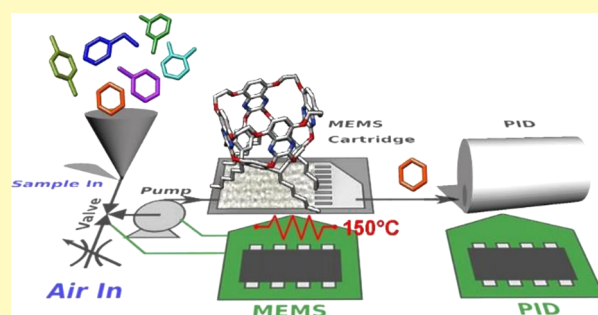
<sup>§</sup>CNR-IMM Bologna, Via P. Gobetti 101, 40129 Bologna, Italy

<sup>||</sup>Dipartimento di Ingegneria e Architettura, Università di Parma, Parco area delle Scienze 181/A, 43124 Parma, Italy

**S** Supporting Information

**ABSTRACT:** In this work we report a comprehensive study leading to the fabrication of a prototype sensor for environmental benzene monitoring. The required high selectivity and ppb-level sensitivity are obtained by coupling a silicon-integrated concentration unit containing the specifically designed EtQxBox cavitant to a miniaturized PID detector. In the resulting stand-alone sensor, the EtQxBox receptor acts at the same time as highly sensitive preconcentrator for BTEX and GC-like separation phase, allowing for the selective desorption of benzene over TEX. The binding energies of the complexes between EtQxBox and BTX are calculated through molecular mechanics calculations. The examination of the corresponding crystal structures confirms the trend determined by computational studies, with the number of C–H···N and CH···π interactions increasing from 6 to 9 along the series from benzene to *o*-xylene. The analytical performances of EtQxBox are experimentally tested via SPME, using the cavitant as fiber coating for BTEX monitoring in air. The cavitant EFs are noticeably higher than those obtained by using the commercial CAR-DVB-PDMS. The LOD and LOQ are calculated in the ng/m<sup>3</sup> range, outperforming the commercial available systems in BTEX adsorption. The desired selective desorption of benzene is achieved by applying a smart temperature program on the EtQxBox mesh, which starts releasing benzene at lower temperatures than TEX, as predicted by the calculated binding energies. The sensor performances are experimentally validated and ppb<sub>v</sub> level sensitivity toward the carcinogenic target aromatic benzene was demonstrated, as required for environmental benzene exposure monitoring in industrial applications and outdoor environment.

**KEYWORDS:** benzene sensor, cavitands, preconcentrators, MEMS device, SPME fiber



Selective monitoring of aromatic volatile organic compounds (VOC) in air, namely, BTEX (benzene, toluene, ethylbenzene and xylenes), is both socially relevant and technologically challenging. Highly selective carcinogenic benzene detection is particularly difficult, due to the concurrent requirements of high selectivity, caused by the presence of overwhelming amounts of other aromatic and aliphatic VOC, and extreme sensitivity (5 μg/m<sup>3</sup> is the present EU limit value for average exposure).<sup>1</sup>

BTEX are generally monitored by passive samplers and successive off-line analyses, resulting in data on averaged exposure levels.<sup>2</sup> Present real-time benzene monitoring systems for in-field environmental applications are bulky and expensive, being automatic high-end systems derived from laboratory instrumentation.<sup>3,4</sup> Recently, miniaturized versions of these systems have been proposed, but they are still limited in terms of response time and high power consumption.<sup>5,6</sup> Simple, low-cost systems based on solid-state gas sensors were recently

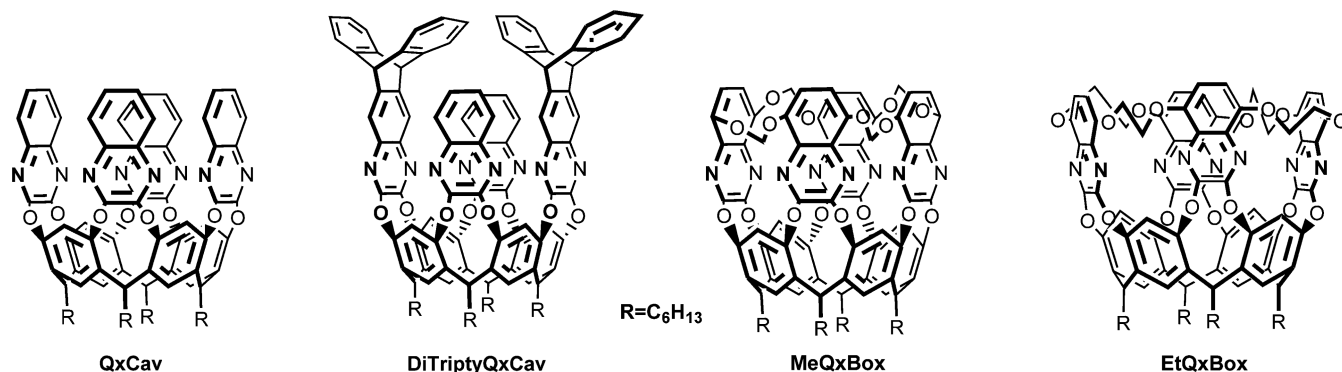
proposed,<sup>7</sup> the most important being metal oxide sensors (MOS), quartz microbalances (QMB), surface acoustic waveguides (SAW), and polymeric sensors.<sup>8</sup> These technologies have often reached sufficient sensitivity for the detection of the target gas species, but generally their selectivity is limited and not sufficient for reliable quantification or early warning systems. Moreover, these are not viable solutions for distributed sensing, i.e., for stand-alone sensors for urban or industrial monitoring and personal warning systems. Multisite monitoring of benzene needs small, low consumption devices without maintenance service (i.e., carrier gas replacements for GC), amenable to be installed across urban and industrial settings. 62

**Received:** February 22, 2017

**Accepted:** March 22, 2017

**Published:** March 22, 2017

Chart 1. Molecular Structure of the Compounds Used in This Study



63 Recently, some companies launched on the market a hand-  
 64 held gas detector, a photoionization detector (PID) equipped  
 65 with a 9.8 eV lamp, with two-mode operation for the rapid  
 66 detection of benzene and total aromatic compounds (TAC).<sup>9</sup>  
 67 The default TAC mode screens out all the aliphatic compounds  
 68 which have an ionization potential higher than 10.0 eV, leaving  
 69 just the TAC whose ionization potential is below 10.0 eV. If the  
 70 TAC measurements exceed safety levels, then the benzene can  
 71 be identified using a prefilter, which contains a strongly  
 72 oxidizing agent, which reacts with all alkylated VOC aromatics,  
 73 except benzene. The detection limit is at ppb<sub>v</sub> levels and the  
 74 humidity interference is minimized using a fence electrode.  
 75 Alternatively, chip measurement systems (CMS) are proposed,  
 76 which can operate at low ppb<sub>v</sub> levels only in the absence of  
 77 humidity.<sup>9</sup> None of these detectors, however, meet the  
 78 stringent environmental limits for benzene detection in air.

79 The exploitation of molecular receptors as sensing materials  
 80 is particularly attractive to address the selectivity issue. The  
 81 progress made in designing synthetic receptors enables the  
 82 modulation of the sensor selectivity toward different classes of  
 83 compounds by mastering the weak interactions occurring  
 84 between the sensing material and the analytes.<sup>10,11</sup>

85 So far, most of the work has focused on receptors for the  
 86 complexation of aromatic compounds in solution.<sup>12–15</sup> Solid  
 87 state recognition of aromatic vapors, with particular emphasis  
 88 on C8 aromatics, has been achieved using porous materials  
 89 such as zeolites,<sup>16</sup> MOFs,<sup>17–19</sup> CD-MOF,<sup>20,21</sup> clathrates,<sup>22</sup> and  
 90 molecular organic cages.<sup>23,24</sup> These systems are shape-selective  
 91 thanks to the presence of well-defined, shape-persistent portals  
 92 in the solid state. As a remarkable example, complete  
 93 discrimination between structural isomers mesitylene and 4-  
 94 ethyltoluene has been achieved.<sup>23</sup> However, shape recognition  
 95 between airborne benzene and toluene turned out to be elusive  
 96 so far, thus jeopardizing environmental monitoring via  
 97 supramolecular sensing.

98 In 2007 we reported an innovative approach to sub-ppb<sub>v</sub>  
 99 level benzene detection in air. A miniaturized system was  
 100 proposed, composed of a selective supramolecular concen-  
 101 tration unit, a Si-micromachined GC column and a Si-  
 102 integrated MOS sensor.<sup>25</sup> The issue of achieving at the same  
 103 time molecular level selectivity and low-ppb<sub>v</sub> sensitivity for  
 104 benzene has been solved by disconnecting the recognition  
 105 element from the detection unit. The recognition event is  
 106 assigned to a quinoxaline cavitand receptor (**QxCav**, **Chart 1**),  
 107 capable of selectively trapping aromatic vapors at the gas–solid  
 108 interface.<sup>26</sup> The selective concentration component is inter-  
 109 faced to the Si-integrated GC column, necessary for the  
 110 separation of the different aromatic compounds released by the

trapping unit, which are then individually channeled to the  
 111 MOS detector.<sup>27</sup> This system has been successfully tested in  
 112 the field. Despite its good performance, this device is rather  
 113 complex and not suited for low-cost distributed sensing,  
 114 because of the need of GC separation of benzene from TEX.  
 115 To overcome this problem, we designed and tested two novel  
 116 quinoxaline cavitands, following two different approaches to  
 117 maximize benzene selectivity: (i) cavity roofing and (ii) cavity  
 118 mouth reduction. In both cases the performances of the  
 119 cavitands were tested using solid-phase micro extraction  
 120 (SPME) as analytical sampling technique. In the first attempt,  
 121 the introduction of two triptycene units at the upper rim  
 122 (**DiTriptyQxCav**, **Chart 1**) enhanced the confinement of  
 123 BTEX within the cavity with respect to the parent **QxCav**.<sup>28</sup> In  
 124 the second case, the introduction of four methylenedioxy bridges  
 125 between the quinoxaline wings (**MeQxBox**, **Chart 1**) provides  
 126 both cavity rigidification and reduction of the cavity opening.  
 127 The result was an exceptional increase in BTEX uptake  
 128 compared to commercial fiber coatings, accompanied by a  
 129 partial bias toward benzene.<sup>29</sup> However, none of the two  
 130 approaches was effective in benzene preferential retention over  
 131 TEX.  
 132

These results prompted us to look at the issue from a  
 133 different perspective, reversing the selectivity scale in favor of  
 134 TEX complexation over benzene inclusion. However, this bias  
 135 must be obtained by strengthening the interactions of TEX  
 136 with the cavitand and not by reducing benzene binding, in  
 137 order to maintain the required preconcentrator sensitivity.  
 138

139 Herein, we report a comprehensive study leading to the  
 140 fabrication of a stand-alone prototype sensor for environmental  
 141 benzene monitoring. The proposed goal has been achieved  
 142 using a specifically designed cavitand, called **EtQxBox** (**Chart**  
 143 **1**), which acts at the same time as selective preconcentrator and  
 144 GC-like separation device. The type and number of the  
 145 interactions of the **EtQxBox** cavity with the aromatic guests has  
 146 been determined in the solid state, while the relative strengths  
 147 of the corresponding complexes were calculated via molecular  
 148 mechanics calculations. The analytical performances of **EtQx-**  
 149 **Box** were then evaluated via SPME and compared with those of  
 150 the other cavitands depicted in **Chart 1**.<sup>29a</sup> Finally, a  
 151 miniaturized benzene monitoring sensor equipped with a  
 152 MEMS cartridge packed with **EtQxBox** was fabricated and  
 153 validated for benzene detection in air.

## RESULTS AND DISCUSSION

154  
 155 **Design and Synthesis of the Cavitand Receptor.** Our  
 156 goal was the design of a macrocyclic host capable to complex

157 aromatic VOC with high efficiency and, at the same time, to  
 158 bind preferentially TEX over benzene. The starting point was  
 159 the understanding of the mechanism of guest uptake/release by  
 160 QxCav at the solid–gas interface. In solution, using a related  
 161 cavitand, Rebek showed that guest release requires a conforma-  
 162 tional opening of the lateral walls, to avoid the prohibitive cost  
 163 of complete cavity desolvation.<sup>30</sup> The fluttering angle of the  
 164 quinoxaline walls in solution has been experimentally evaluated  
 165 by Diederich and co-workers using FRET:<sup>31</sup> the average value  
 166 of 16° is in line with the 0–29° range determined by Sum-  
 167 Frequency Vibrational Spectroscopy measurements on a  
 168 QxCav monolayer.<sup>32</sup> This last measurement, coupled with  
 169 theoretical calculations, indicates that the QxCav cavity is  
 170 “breathing” in the solid state. It is reasonable to assume that the  
 171 breathing is amplified increasing the temperature.

172 Since solvation is absent in the solid state, our reasoning was  
 173 that limiting the breathing of the cavity would boost the guest  
 174 uptake by filling the empty cavity and thermally stabilize the  
 175 resulting complex. To this purpose we designed an EtQxBx  
 176 cavitand, in which the three different, well-separated rims of  
 177 electron-rich surfaces are preorganized for weak intermolecular  
 178 attractive interactions with the aromatic guests (Figure 1).

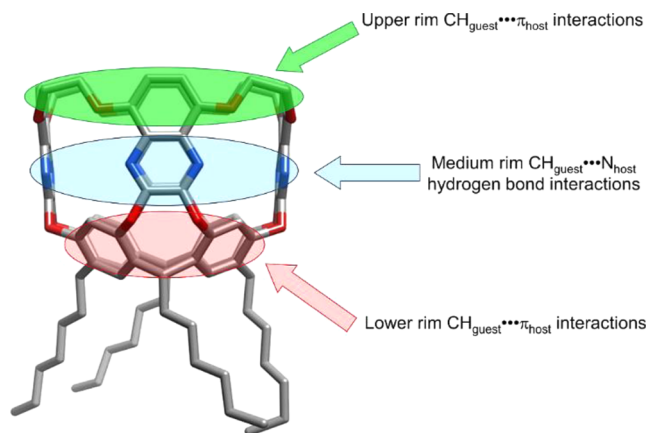


**Figure 1.** Chemical structure of the EtQxBx host cavitand with lower, medium, and upper rim interaction sites, highlighted in different colors.

179 The rationale of this design can be summarized as follows:  
 180 (a) at the lower rim, the four aromatic surfaces of the  
 181 resorcinarene skeleton can interact with two “bottom” C–H  
 182 groups of benzene, toluene or xylenes via C–H... $\pi$  interactions;  
 183 (b) at the medium rim, the nitrogen atoms of the quinoxaline  
 184 rings can act as hydrogen bond acceptors toward the two  
 185 “equatorial” C–H groups of benzene, toluene, or xylenes; (c) at  
 186 this point, the role of the aromatic surfaces at the upper rim of  
 187 the cavitand becomes crucial for selectivity. In fact, these  
 188 surfaces, too far to interact with benzene, become available for  
 189 attractive intermolecular C–H... $\pi$  interactions with one or two  
 190 methyl groups in the case of toluene and xylenes, respectively.

191 It is thus to be expected that the host–guest binding energy  
 192 increases as the number of the attractive interactions increases,  
 193 with xylenes, ethylbenzene, and toluene bound more strongly  
 194 than benzene. To prove this hypothesis, host–guest  
 195 interactions in the solid state were analyzed studying the  
 196 crystal structures of three BTX complexes with EtQxBx; the  
 197 relative strength of the same complexes was obtained in the gas  
 198 phase by molecular modeling calculations. Partial rigidification

of the lateral walls in cavitands has been already reported by  
 Diederich<sup>33</sup> and Rebek,<sup>34</sup> while Bruce Gibb<sup>15</sup> reported the  
 preparation of larger, fully blocked deep-cavity cavitands. In our  
 design, the connecting units at the upper rim should not alter  
 cavity shape and depth, to avoid variations in the cavity affinity  
 for aromatic hydrocarbons. Therefore, we opted for introducing  
 ethylenedioxy units connecting the quinoxaline rings laterally.  
 EtQxBx was obtained following a three-step procedure. First,  
 the hexyl-footed resorcinarene was 4-fold bridged with 2,3-  
 dichoro-5,8-dimethoxy quinoxaline under microwave irradiation,  
 leading to octamethoxy QxCav 1 (Scheme S1, SI). Then,  
 the eight methyl groups on the quinoxaline flaps were removed  
 using AlCl<sub>3</sub> in dry toluene to afford the corresponding  
 octahydroxy QxCav 2.<sup>29b</sup> Finally the two-by-two bridging of  
 the four hydroxyl pairs with ethylene di(*p*-toluenesulfonate)  
 afforded EtQxBx cavitand in 44% overall yield (Scheme S1,  
 SI). EtQxBx in solution adopts a rigid vase conformation, as  
 testified by the 5.79 ppm resonance of the diagnostic  
 resorcinarene bridging methyne (Figure S1, SI).

**Gas-Phase Molecular Simulation for EtQxBx Complexes.** We carried out molecular mechanics calculations using the MMFF94 Merck molecular force field,<sup>35</sup> which has excellent parametrization of van der Waals and electrostatic intermolecular interactions (comparable with those obtainable with HF/6-31G\* calculations).

The calculated geometries and binding energies of the three complexes are shown in Figure 2, together with the weak attractive intermolecular host–guest interactions represented by green lines. The nature of the intermolecular interactions and their calculated geometrical parameters are summarized in Tables S3–S5. The calculations predict that complexation of benzene occurs via two C–H... $\pi$  interactions (entries 1,2) and two bifurcated C–H...N hydrogen bonds (entries 3–6).

No other host–guest attractive interactions are possible in the case of benzene and the calculated binding energy is  $\Delta E = -71.62$  (kJ/mol). The binding energy increases ( $\Delta E$  becomes more negative:  $-76.26$  kJ/mol) in the toluene@EtQxBx complex due to the increased number of the host–guest interactions: eight over six, due to the formation of two additional C–H... $\pi$  interactions (entries 7,8) involving the methyl group of toluene and the aromatic surfaces at the upper rim of EtQxBx. The calculations also predict that *o*-xylene is the preferred guest due to the formation of the additional host–guest C–H... $\pi$  interaction (entry 9) involving the second methyl group present in *o*-xylene. This increases the binding to  $\Delta E = -79.98$  (kJ/mol) demonstrating the crucial role of the conformationally blocked aromatic surfaces at the upper rim of the host to achieve the expected scale of selectivity among the three guests.

**Solid-State Inclusion.** In order to experimentally verify the in silico simulations, we studied the inclusion ability of EtQxBx toward BTEX by different crystallization experiments, dissolving the cavitand in DMSO and adding benzene, toluene, and *o*-xylene, respectively. In all cases, single crystals suitable for X-ray diffraction analysis were obtained by slow evaporation. The examination of the three crystal structures evidence that all the aromatic compounds are positioned within the host cavity, and that the resulting intermolecular interactions follow the trend observed in the computational studies, with the number of interactions increasing along the series from benzene to *o*-xylene. In the molecular structure of benzene@EtQxBx, the asymmetric unit comprises two cavitands differing one from the other for the orientation of the alkyl legs. In both the hosts,

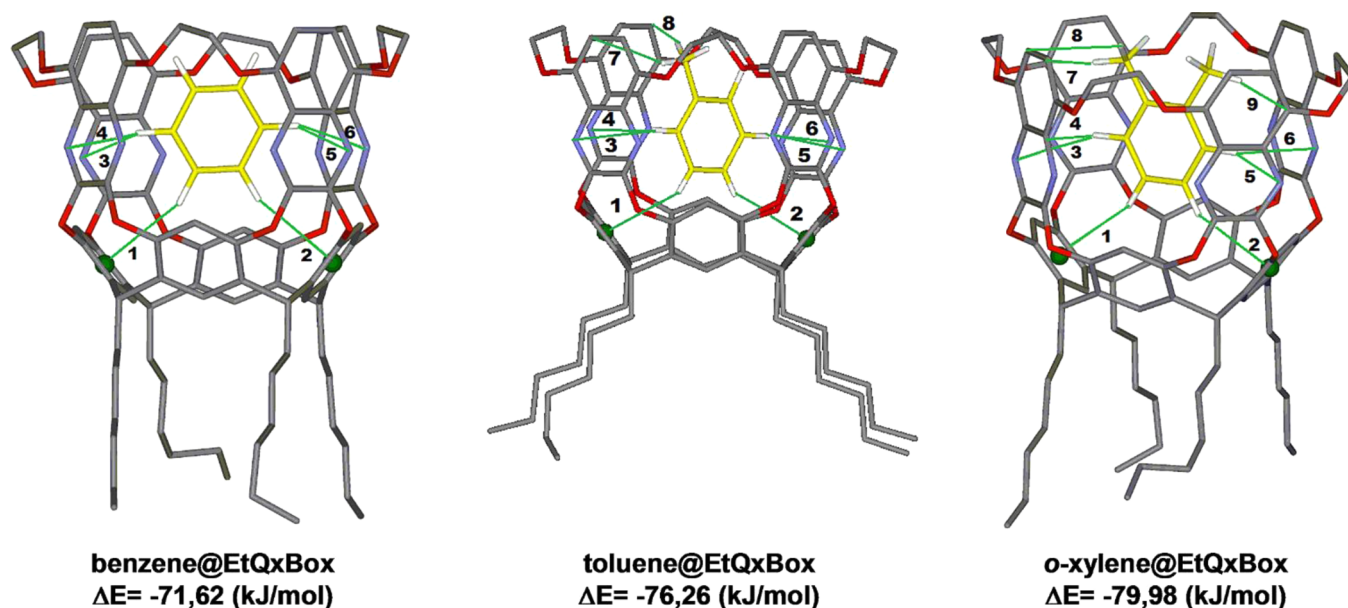


**Figure 2.** Stick views of the three complexes. Colors: C, gray (C atoms of the guest; yellow); O, red; N, cyan; H, white. Only the guest hydrogen atoms have been shown for clarity. Intermolecular host–guest interactions are represented as green lines.

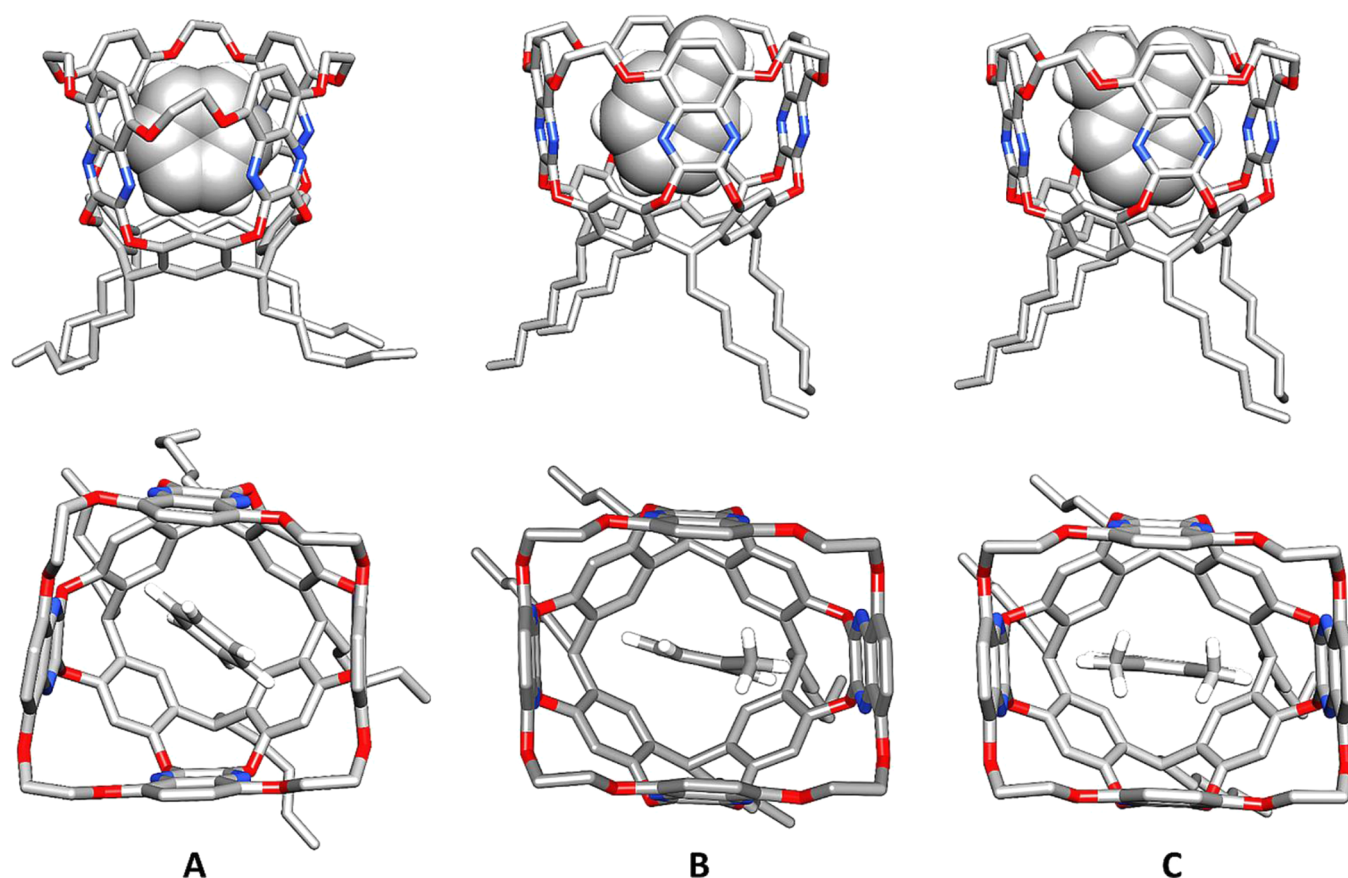


**Figure 3.** Side and top view of the molecular structures of **benzene@EtQxBox** (A), **toluene@EtQxBox** (B), and **o-xylene@EtQxBox** (C). Only the hydrogen atoms of the guest are shown. Benzene and DMSO solvent molecules have been omitted for clarity.

262 benzene is included deeply within the cavity (see Figure 3A,  
263 only one of the two independent cavitands is shown), forming  
264 six weak noncovalent interactions (for the geometrical  
265 parameters see Table S3): two C–H... $\pi$  interactions with the  
266 lower aromatic bowl of the cavitand, and two bifurcated C–H...  
267 N interactions with the nitrogen atoms of two adjacent

quinoxaline moieties, as shown in Figure 2. Indeed, the number  
268 and types of interactions in the calculated and in the solid state  
269 structure of the complex are the same, even if the benzene guest  
270 has a slightly different inclination in the two cases (see Figure  
271 S5). The self-assembly of the complexes in the crystal lattice is  
272 assisted by several benzene and DMSO solvent molecules 273

274 which fill the voids available. Also in the molecular structure of  
 275 **toluene@EtQxBox** (Figure 3B), two C–H $\cdots\pi$  interactions  
 276 with the lower rim of the cavitand and two bifurcated C–H $\cdots$ N  
 277 interactions with the two nitrogen atoms of the same  
 278 quinoxaline ring have been observed. However, the global  
 279 orientation of the guest differs from that of benzene, being  
 280 parallel to two quinoxaline walls of the cavitand, to maximize  
 281 the interactions with the cavity. This orientation allows the  
 282 methyl group, which is disordered over two equivalent  
 283 positions, to form C–H $\cdots\pi$  interactions with the conforma-  
 284 tionally blocked aromatic rings at the upper rim of the cavitand,  
 285 again in good agreement with the calculated data. The  
 286 geometrical parameters for the two disordered C–H $\cdots\pi$   
 287 interactions are reported in Table S4 (see SI). *o*-Xylene  
 288 behaves essentially like toluene, yielding the complex *o*-  
 289 **xylene@EtQxBox**, which is perfectly comparable in geometry  
 290 and host–guest interactions to the toluene analogue (Figure  
 291 3C). In this case no disorder occurs, and the two *ortho* methyl  
 292 groups are both involved in equivalent CH $\cdots\pi$  interactions (see  
 293 parameters in Table S5, SI). This additional interaction  
 294 accounts for the increased complexation binding energy  
 295 calculated in the gas phase for the *o*-xylene@EtQxBox  
 296 complex.

297 **Solid-Phase Microextraction Analysis (SPME).** In order  
 298 to test the capabilities of the cavitand toward BTEX trapping,  
 299 an **EtQxBox** SPME coating was developed and characterized.  
 300 Preliminary investigations by thermogravimetric analyses were  
 301 performed on **EtQxBox** in air to determine its decomposition  
 302 temperature and its long-term thermal stability under the  
 303 required desorption temperatures. **EtQxBox** is stable in air up  
 304 to 400 °C (Figure S8, SI) and it shows an excellent thermal  
 305 stability at 250 °C for over 15 h (Figure S9, SI). The  
 306 introduction of the four ethylendioxy bridging groups does not  
 307 reduce the thermal stability of the receptor with respect to the  
 308 parent **QxCav**.<sup>36</sup> The thermal stability of the coating was also  
 309 evaluated by conditioning the SPME fibers in the GC injector  
 310 port at 250 °C for 2 min: no significant bleeding was observed,  
 311 thus confirming the high thermal resistance of the material.

312 Scanning electron microscopy of the coated SPME fiber  
 313 showed a homogeneous and uniform distribution of the  
 314 cavitand all along the fiber with a coating thickness of  $40 \pm 6$   
 315  $\mu\text{m}$  (Figure S10, SI). The effectiveness of **EtQxBox** fiber in  
 316 BTEX sampling was tested by SPME-GC-MS. The analysis of  
 317 an air mixture containing an amount of aliphatic hydrocarbons  
 318 (from C6 to C9) 2 orders of magnitude higher than BTEX  
 319 ( $38\text{--}56 \mu\text{g}/\text{m}^3$  vs  $385\text{--}473 \text{ ng}/\text{m}^3$  range), proved that the  
 320 aromatic analytes are strongly retained into the **EtQxBox** cavity  
 321 and can be exhaustively desorbed at temperatures higher than  
 322 250 °C (Figure S11, SI). These findings are in agreement with  
 323 the X-ray data, confirming the complexation of the analytes into  
 324 the cavity. By contrast aliphatic hydrocarbons are completely  
 325 removed at 50 °C, being only physisorbed in the solid (Figure  
 326 S11, SI). Repeatability of data, in terms of both intra- and  
 327 intermediate precision, was assessed by performing 5 replicated  
 328 measurements along 2 weeks obtaining relative standard  
 329 deviations (RSD) always lower than 9%.

330 The enrichment capabilities toward BTEX were also  
 331 evaluated in terms of enrichment factors (EFs).<sup>37</sup> EFs were  
 332 calculated as the ratio of the concentration of the analyte in the  
 333 fiber after the extraction to that of the analyte in the gas  
 334 standard mixture. As shown in Figure 4, the cavitand EFs were  
 335 noticeably higher than those obtained by using the commercial  
 336 CAR-DVB-PDMS 2 cm–50/30  $\mu\text{m}$  fiber. In particular, the EFs

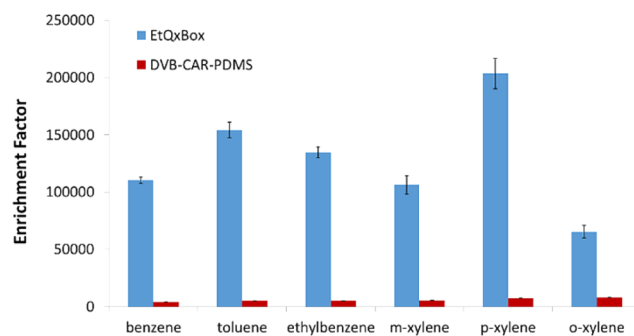


Figure 4. Enhancement factors per coating thickness of the **EtQxBox** fiber for BTEX extraction. HS-SPME conditions: extraction time 15 min, 25 °C (3 replicates).

were up to 30 times higher than those obtained using the  
 commercial fiber. These findings suggested the use of **EtQxBox**  
 for the development of portable devices in which the cavitand is  
 used as trapping material for the online and in situ  
 environmental monitoring of BTEX. Limits of detection  
 (LOD, Table 1) and limits of quantitation (LOQ, Table S8,  
 SI) in the low  $\text{ng}/\text{m}^3$  range proved the capabilities of the  
**EtQxBox** as adsorbent for the determination of BTEX in air at  
 trace levels. Finally, the calculated LODs were compared with  
 those achieved both by commercially devices used for air  
 quality monitoring and by supramolecular receptors already  
 developed by our research group, i.e., tetraquinoxaline cavitands  
 functionalized at the upper rim with four methyldioxy  
 bridges (**MeQxBox**)<sup>29</sup> and two triptycene moieties (**DiTripty-  
 QxCav**),<sup>28</sup> respectively (Table 1).

As reported in Table 1, both conformationally blocked  
 quinoxaline-based cavitand receptors showed better perform-  
 ance in terms of sensitivity compared to systems commonly  
 used for air monitoring like Radiello. The same behavior was  
 observed toward both high-end apparatus based on optical  
 fibers and commercial SPME fibers like DVB-CAR-PDMS.  
 Additional advantages rely on both the use of shorter extraction  
 times, thus speeding up BTEX monitoring, and the enhanced  
 selectivity toward aromatic hydrocarbons as already demon-  
 strated by our previous studies.<sup>28,29b</sup>

The comparison of the SPME extraction performances of  
**MeQxBox** and **EtQxBox** allows one to single out the effect of  
 the length of the bridging units among the quinoxaline walls.  
 The shorter methyldioxy units reduce the cavity mouth  
 entrance leading to the lowest LOD for benzene at the expense  
 of BTEX desorption selectivity. Therefore, the size of the cavity  
 mouth in the **QxBox** series is pivotal to modulate the thermal  
 release of the various aromatic guests.

**Sensor Manufacturing and Benzene Detection.** A  
 simple device for benzene monitoring based on **EtQxBox** for  
 BTEX preconcentration and selective benzene desorption into  
 a miniaturized photoionization detector (Mini-PID PPB by  
 IonScience) was designed and tested under laboratory  
 conditions. Compared to the mini-GC device developed by  
 us in 2009,<sup>27</sup> the use of **EtQxBox** instead of **QxCav** allows for  
 combining the preconcentration and the GC separation  
 capabilities into a single MEMS chip packed with 10 mg of a  
 proper mesh of **EtQxBox** cavitand.

In fact, the selectivity between benzene and the other  
 aromatics is achieved by applying a smart temperature program  
 on the **EtQxBox** mesh, which starts releasing benzene at lower  
 temperatures than toluene and xylene, as predicted by the 383

**Table 1.** Comparison between the LOD Values ( $\text{ng}/\text{m}^3$ ) of the Supramolecular Receptors and the Commercially Available Devices

	EtQxBOX	MeQxBOX	DiTriptyQxCav	QxCav	DVB-CAR-PDMS	RADIELLO	optical fiber <sup>38</sup>
extraction time	(15 min) <sup>a</sup>	(15 min) <sup>a</sup>	(15 min) <sup>a</sup>	(15 min) <sup>a</sup>	(15 min) <sup>a</sup>	(24 h) <sup>a</sup>	(25 min) <sup>a</sup>
benzene	0.7	0.4	1.7	5.2	17.1	290	1.6
toluene	0.4	0.6	3.1	7.2	2.1	90	1.5
ethylbenzene	0.4	0.5	1.3	5.7	4.8	40	1.2
<i>m</i> -xylene	0.8	1.2	2.0	10.0	6.1	70	1.3
<i>p</i> -xylene	0.3	0.6	1.3	9.0	6.1	80	1.7
<i>o</i> -xylene	0.5	1.0	2.2	12.5	14.3	10	2.0

<sup>a</sup>Extraction time used in each study.

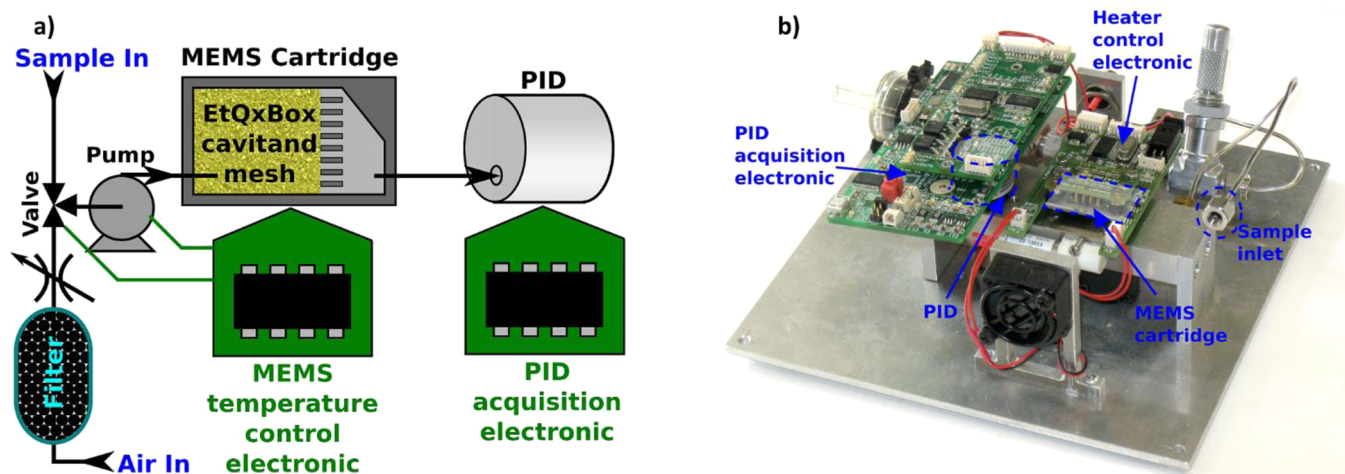


**Figure 5.** Schematic representation of the benzene monitoring device (a) and photograph of the prototype (b) with an inset showing the MEMS chip packed with EtQxBox.

384 calculated binding energies  $\Delta E$ . Under these conditions, the use  
385 of a temperature desorption ramp replaces the GC minicolumn.

386 The fabrication process for the packed MEMS preconcentrators  
387 was reported previously.<sup>27</sup> Figure 5a shows a schematic  
388 representation of the device, while Figure 5b shows a  
389 photograph of the prototype used for this work. The  
390 interconnections between the single components are made  
391 through a stainless steel block with suitable machining, which  
392 mounts a pump (KNF Neuberger model NMP09B), a bistable  
393 3-way microvalve (by The Lee Company), the PID, and the  
394 MEMS chip.

395 The sampling step consists of pumping the sample at a flow  
396 of up to 120 mL/min into the MEMS chip. The duration and  
397 flow rate of the sampling step can be adapted to specific  
398 applications, and different configurations were tested. In  
399 particular, with long sample times (50 min) at higher flow  
400 rates (120 mL/min) ppb<sub>v</sub>-level sensitivity to benzene was  
401 demonstrated. For the injection/separation step, the 3-way  
402 valve is switched and an activated carbon filter is used to  
403 provide clean air into the MEMS, which is heated at a rate of  
404  $>50$  °C/s to release the sampled aromatics. The flow during the  
405 separation phase can be regulated by means of a needle-valve,  
406 and several flow-rates were tested. The best results in terms of  
407 selectivity to benzene over toluene were found with a 30 mL/  
408 min flow. Figure 6 shows some typical signals acquired by the  
409 PID detector during the desorption temperature ramp. In these  
410 plots, the MEMS cartridge filled with EtQxBox was kept at  
411 room temperature using the pump to sample the test mixture  
412 from the sample inlet at 120 mL/min up to  $t = 5$  min, when the

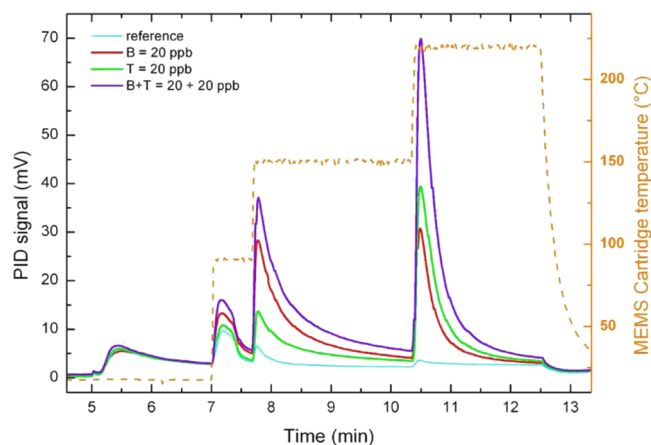


**Figure 6.** Typical responses of the PID detector to a temperature ramp for benzene (B, red), toluene (T, green), and a mixture of benzene and toluene (B+T, purple), compared to a “reference” sample of only air (cyan).

413 valve was switched to the filter line with a reduced flow of 30  
414 mL/min.

415 Starting at  $t = 7$  min, the temperature was increased to 90 °C  
416 for 40 s to release any nonspecifically adsorbed species. The  
417 next temperature step at 150 °C is applied to release  
418 preferentially benzene. As can be seen from the plots, the  
419 “reference” injection (only air, cyan line) results in a very small  
420 signal, while the injection of 20 ppb<sub>v</sub> of benzene yields a  
421 relevant peak (red line), which is only slightly smaller than the  
422 peak of 20 ppb<sub>v</sub> benzene + 20 ppb<sub>v</sub> toluene (purple line).

423 This first result demonstrates how only a very small amount  
 424 of toluene is released at 150 °C (see green line, 20 ppb<sub>v</sub> of  
 425 toluene only). This first temperature step is the most significant  
 426 for benzene quantification, since toluene interferes only slightly  
 427 during the 150 °C step. During the next temperature step at  
 428 220 °C, more toluene (green) than benzene (red) is released. It  
 429 is evident that the separation between benzene and toluene is  
 430 not complete, due to the very short cartridge used for this work.  
 431 Nevertheless, by calibrating the system and using a simple  
 432 linear combination of the responses at the two temperatures  
 433 (150 and 220 °C), the small signal generated by toluene at the  
 434 150 °C step can be easily subtracted (see SI for more details),  
 435 and a very good prediction of the benzene concentration in  
 436 mixtures with much higher toluene concentrations can be  
 437 achieved, as shown in Figure 7. The data reported in Figure 7

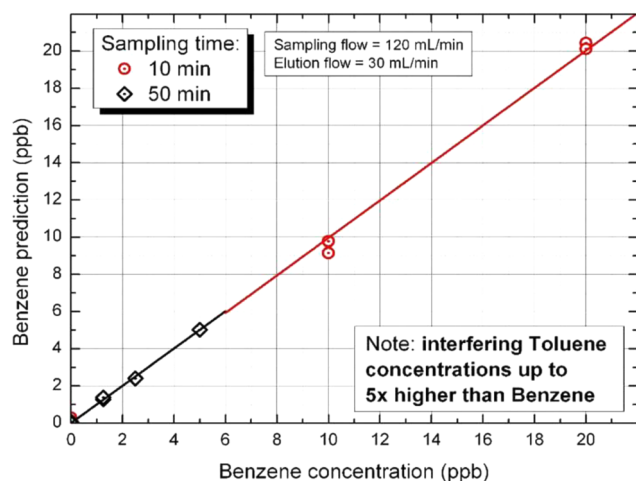


Figure 7. Benzene concentrations calculated using the equations (eqs 1a and 1b in SI) on a set of measurements performed with the prototype shown in Figure 5b. These values were calculated on samples where interfering toluene concentrations were up to 5 times higher than the benzene concentration.

438 refers to a campaign of 36 measurements where benzene  
 439 concentrations between 1.25 and 20 ppb<sub>v</sub> were injected  
 440 together with interfering toluene concentrations which were  
 441 up to 5 times higher than the benzene concentrations, to prove  
 442 the good prediction capability of the proposed sensor device.

443 The selectivity of benzene toward toluene, as shown in  
 444 Figure 6, is expected to be improved in future works by using a  
 445 longer MEMS cartridge filled with the EtQxBox, to increase the  
 446 separation effect. Nevertheless, the current implementation has  
 447 already demonstrated the capability of selectively quantifying  
 448 benzene with a detection range spanning from 1.25 to 20 ppb<sub>v</sub>.  
 449 The superior benzene complexation capabilities of EtQxBox  
 450 versus the previously reported QxCav can be disclosed from  
 451 the plots of Figure 8, where the effect of the temperature during  
 452 the sampling step is compared for the two cavitands. For both  
 453 plots, the sensitivity is normalized to the value of 20 °C,  
 454 resulting in arbitrary units on the y-axis. At temperatures  
 455 slightly higher than 20 °C, QxCav rapidly decreases the  
 456 complexation efficiency in adsorption, while EtQxBox has the  
 457 same preconcentration capabilities up to temperatures close to  
 458 60 °C, while around 100 °C the beginning desorption regime is  
 459 evident. This widens the working temperature regime available  
 460 for the corresponding device a lot. These findings demonstrate  
 461 that the presence of a conformationally blocked cavity is able to

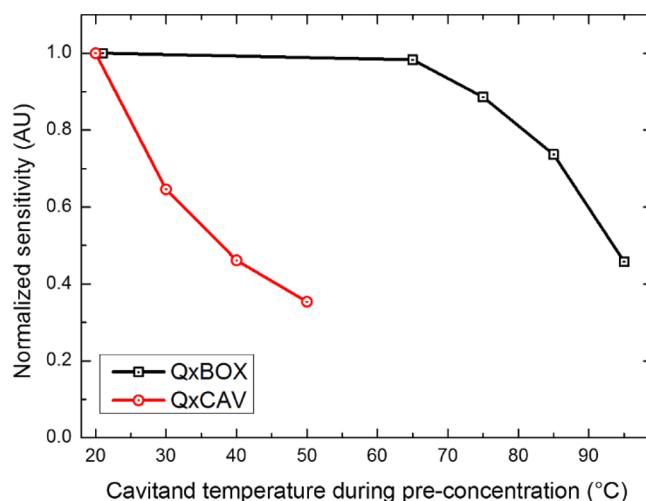


Figure 8. Normalized sensitivity toward benzene at increasing temperatures compared for QxCav (red line) and EtQxBox (black line). The higher binding energy of EtQxBox results in the capability of preconcentrating benzene efficiently up to over 60 °C.

strengthen the host–guest interactions, thus increasing the  
 selectivity of the proposed device.

## CONCLUSIONS

This work describes a new sensor for ppb level detection of benzene in air, in which high selectivity and extremely high sensitivity are obtained by coupling a MEMS-integrated supramolecular concentration unit to a miniaturized PID detector. By mastering molecular recognition at the gas–solid interface we have been able to produce a stand-alone sensor, in which the cavitant receptor EtQxBox acts at the same time as selective preconcentrator and GC-like separation device. EtQxBox is capable of selectively trapping BTEX at the ng/m<sup>3</sup> level within its conformationally rigid cavity delimited by four quinoxaline walls linked via ethylenedioxy bridges. The conformational rigidity of the cavitant maximizes the binding of TEX with respect to benzene by increasing the number of synergistic CH $\cdots\pi$  interactions in the latter. With respect to previous cavitands used for the selective benzene detection and quantification, EtQxBox features an enhanced overall BTEX trapping efficiency, while the different binding energies for the single aromatics are responsible of the GC-like separation. These characteristics allows for the fabrication of a simplified detection system, in which a single MEMS device provides high efficiency preconcentration and BTEX separation capabilities. It is noteworthy that the ppb<sub>v</sub>-level sensitivity was demonstrated with a simple, stand-alone, and unsupervised sensing device, autonomously sampling and analyzing the test samples. In perspective, EtQxBox is the preconcentrator of choice to build a highly efficient stand-alone sensor for personal benzene exposure monitoring in industrial settings.

## ASSOCIATED CONTENT

### Supporting Information

The Supporting Information is available free of charge on the ACS Publications website at DOI: 10.1021/acssensors.7b00110.

Experimental procedures and characterization (Scheme S1, Figure S1); supporting crystallographic data (Tables S1–S2–S6–S7, Figures S2–S7); MMFF94 Merck

500 molecular force field calculations (Tables S3–S4–S5);  
501 TGA analyses (Figures S8–S9); fiber characterization  
502 (Figure S10). SPME analysis (Figure S11); GC/MS  
503 analysis (Table S8); system calibration and prediction of  
504 benzene concentration (eqs 1a-b and 2a-b) (PDF)

## 505 ■ AUTHOR INFORMATION

### 506 Corresponding Author

507 \*E-mail: [enrico.dalcanale@unipr.it](mailto:enrico.dalcanale@unipr.it).

### 508 ORCID

509 Roberta Pinalli: 0000-0002-0000-8980

510 Alessandro Pedrini: 0000-0003-3949-7563

511 Federica Bianchi: 0000-0001-7880-5624

512 Enrico Dalcanale: 0000-0001-6964-788X

### 513 Present Address

514 #Dipartimento di Scienze Chimiche, Università di Padova, via  
515 Marzolo 1, 35131 Padova.

### 516 Author Contributions

517 All authors have given approval to the final version of the  
518 manuscript.

### 519 Notes

520 The authors declare no competing financial interest.

## 521 ■ ACKNOWLEDGMENTS

522 This work was supported by the EU through Projects  
523 FINELUMEN (FP7-ITN-2008-215399) and DIRAC (FP7-  
524 SEC-2009-242309). We acknowledge the Centro Interfacoltà di  
525 Misure “G. Casnati” of the University of Parma for the use of  
526 NMR and HR-MS facilities.

## 527 ■ REFERENCES

528 (1) Directive 2008/50/EC of the European Parliament and of the  
529 Council of 21 May 2008 on ambient air quality and cleaner air for  
530 Europe ([http://ec.europa.eu/environment/air/quality/legislation/  
531 existing\\_leg.htm](http://ec.europa.eu/environment/air/quality/legislation/existing_leg.htm)).

532 (2) Górecki, T.; Namieśnik, J. Passive sampling. *TrAC, Trends Anal.*  
533 *Chem.* **2002**, *21*, 276–291.

534 (3) Daughtrey, E. H., Jr.; Oliver, K. D.; Adams, J. R.; Kronmiller, K.  
535 G.; Lonneman, W. A.; McClenny, W. A. A comparison of sampling  
536 and analysis methods for low-ppb levels of volatile organic  
537 compounds in ambient air. *J. Environ. Monit.* **2001**, *3*, 166–174.

538 (4) Ueno, Y.; Horiuchi, T.; Niwa, O. Air-Cooled Cold Trap Channel  
539 Integrated in a Microfluidic Device for Monitoring Airborne BTEX  
540 with an Improved Detection Limit. *Anal. Chem.* **2002**, *74*, 1712–1717.

541 (5) Liaud, C.; Nguyen, N.; Nasreddine, R.; LeCalvé, S. Experimental  
542 performances study of a transportable GC-PID and two thermo-  
543 desorption based methods coupled to FID and MS detection to assess  
544 BTEX exposure at sub-ppb level in air. *Talanta* **2014**, *127*, 33–42.

545 (6) Jian, R.-S.; Huang, Y.-S.; Lai, S.-L.; Sung, L.-Y.; Lu, C.-J. Compact  
546 instrumentation of a  $\mu$ -GC for real time analysis of sub-ppb VOC  
547 mixtures. *Microchem. J.* **2013**, *108*, 161–167.

548 (7) Bourgeois, W.; Romain, A.-C.; Nicolas, J.; Stuetz, R. M. The use  
549 of sensor arrays for environmental monitoring: interests and  
550 limitations. *J. Environ. Monit.* **2003**, *5*, 852–860.

551 (8) Arshak, K.; Moore, E.; Lyons, G. M.; Harris, J.; Clifford, S. A  
552 review of gas sensors employed in electronic nose applications. *Sens.*  
553 *Rev.* **2004**, *24*, 181–198.

554 (9) AFC International; [http://www.afcintl.com/our-products/gas-  
555 detection-instruments/gas-detectors/gas-specific-detectors/benzene-  
556 gas-detectors.aspx](http://www.afcintl.com/our-products/gas-detection-instruments/gas-detectors/gas-specific-detectors/benzene-gas-detectors.aspx).

557 (10) Lavigne, J. J.; Anslyn, E. V. Sensing A Paradigm Shift in the Field  
558 of Molecular Recognition: From Selective to Differential Receptors.  
559 *Angew. Chem., Int. Ed.* **2001**, *40*, 3118–3130.

(11) Pirondini, L.; Dalcanale, E. Molecular recognition at the gas–  
560 solid interface: a powerful tool for chemical sensing. *Chem. Soc. Rev.* **2007**, *36*, 695–706.

(12) Diederich, F. *Cyclophanes*; The Royal Society of Chemistry:   
563 Cambridge, UK, 1991.

(13) Rebek, J., Jr. Simultaneous Encapsulation: Molecules Held at  
564 Close Range. *Angew. Chem., Int. Ed.* **2005**, *44*, 2068–2078.

(14) Barnes, J. C.; Juríček, M.; Strutt, N. L.; Frascioni, M.; Sampath,  
565 S.; Giesener, M. A.; McGrier, P. L.; Bruns, C. J.; Stern, C. L.; Sarjeant,  
566 A. A.; Stoddart, J. F. ExBox: A Polycyclic Aromatic Hydrocarbon  
567 Scavenger. *J. Am. Chem. Soc.* **2013**, *135*, 183–192.

(15) Jordan, J. H.; Gibb, B. C. Molecular containers assembled  
571 through the hydrophobic effect. *Chem. Soc. Rev.* **2015**, *44*, 547–585.

(16) Kulprathipanja, S.; James, R. B. In *Zeolites in Industrial*  
573 *Separation and Catalysis*; Kulprathipanja, S. Ed.; Wiley-VCH, 2010;  
574 pp 173–202.

(17) Li, J.-R.; Sculley, J.; Zhou, H.-C. Metal–Organic Frameworks  
575 for Separations. *Chem. Rev.* **2012**, *112*, 869–932.

(18) Huang, W.; Jiang, J.; Wu, D.; Xu, J.; Xue, B.; Kirillov, A. M. A  
578 Highly Stable Nanotubular MOF Rotator for Selective Adsorption of  
579 Benzene and Separation of Xylene Isomers. *Inorg. Chem.* **2015**, *54*,  
580 10524–10526.

(19) Cheng, J.-Y.; Wang, P.; Ma, J.-P.; Liu, Q.-K.; Dong, Y.-B. A  
582 nanoporous Ag(I)-MOF showing unique selective adsorption of  
583 benzene among its organic analogues. *Chem. Commun.* **2014**, *50*,  
584 13672–13675.

(20) Holcroft, J. M.; Hartlieb, K. J.; Moghadam, P. Z.; Bell, J. G.;  
586 Barin, G.; Ferris, D. P.; Bloch, E. D.; Algaradah, M. M.; Nassar, M. S.;  
587 Botros, Y. Y.; Thomas, K. M.; Long, J. R.; Snurr, R. Q.; Stoddart, J. F.  
588 Carbohydrate-Mediated Purification of Petrochemicals. *J. Am. Chem.*  
589 *Soc.* **2015**, *137*, 5706–5719.

(21) Hartlieb, K. J.; Holcroft, J. M.; Moghadam, P. Z.; Vermeulen, N.  
591 A.; Algaradah, M. M.; Nassar, M. S.; Botros, Y. Y.; Snurr, R. Q.;  
592 Stoddart, J. F. CD-MOF: A Versatile Separation Medium. *J. Am. Chem.*  
593 *Soc.* **2016**, *138*, 2292–2301.

(22) Lusi, M.; Barbour, L. J. Solid-vapor sorption of xylenes:  
595 prioritized selectivity as a means of separating all three isomers using a  
596 single substrate. *Angew. Chem., Int. Ed.* **2012**, *51*, 3928–3931.

(23) (a) Mitra, T.; Jelfs, K. E.; Schmidtman, M.; Ahmed, A.; Chong,  
598 S. Y.; Adams, D. J.; Cooper, A. I. Molecular shape sorting using  
599 molecular organic cages. *Nat. Chem.* **2013**, *5*, 276–281. (b) Jie, K.; Liu,  
600 M.; Zhou, Y.; Little, M. A.; Bonakala, S.; Chong, S. Y.; Stephenson, A.;  
601 Chen, L.; Huang, F.; Cooper, A. I. Styrene Purification by Guest-  
602 Induced Restructuring of Pillar[6]arene. *J. Am. Chem. Soc.* **2017**, *139*,  
603 2908.

(24) Brutschy, M.; Schneider, M. W.; Mastalerz, M.; Waldvogel, S. R.  
605 Porous Organic Cage Compounds as Highly Potent Affinity Materials  
606 for Sensing by Quartz Crystal Microbalances. *Adv. Mater.* **2012**, *24*,  
607 6049–6052.

(25) Zampolli, S.; Betti, P.; Elmi, I.; Dalcanale, E. A supramolecular  
609 approach to sub-ppb aromatic VOC detection in air. *Chem. Commun.*  
610 **2007**, 2790–2792.

(26) Condorelli, G. G.; Motta, A.; Favazza, M.; Gurrieri, E.; Betti, P.;  
612 Dalcanale, E. Molecular recognition of halogen-tagged aromatic VOCs  
613 at the air–silicon interface. *Chem. Commun.* **2010**, *46*, 288–290.

(27) Zampolli, S.; Elmi, I.; Mancarella, F.; Betti, P.; Dalcanale, E.;  
615 Cardinali, G. C.; Severi, M. Real-time monitoring of sub-ppb  
616 concentrations of aromatic volatiles with a MEMS-enabled mini-  
617 aturized gas-chromatograph. *Sens. Actuators, B* **2009**, *141*, 322–328.

(28) Bertani, F.; Riboni, N.; Bianchi, F.; Brancatelli, G.; Sterner, E. S.;  
619 Pinalli, R.; Geremia, S.; Swager, T. M.; Dalcanale, E. Triptycene-  
620 Roofed Quinoxaline Cavitands for the Supramolecular Detection of  
621 BTEX in Air. *Chem. - Eur. J.* **2016**, *22*, 3312–3319.

(29) (a) Trzcinski, J. W.; Pinalli, R.; Bianchi, F.; Massera, C.;  
623 Dalcanale, E. European Patent No. EP2924041A1, July 27, 2016.  
624 (b) Riboni, N.; Trzcinski, J. W.; Bianchi, F.; Massera, C.; Pinalli, R.;  
625 Sidisky, L.; Dalcanale, E.; Careri, M. Conformationally blocked  
626 quinoxaline cavitand as solid-phase microextraction coating for the  
627 selective detection of BTEX in air. *Anal. Chim. Acta* **2016**, *905*, 79–84.

- 629 (30) Rudkevich, D. M.; Hilmersson, G.; Rebek, J., Jr. Intramolecular  
630 Hydrogen Bonding Controls the Exchange Rates of Guests in a  
631 Cavitand. *J. Am. Chem. Soc.* **1997**, *119*, 9911–9912.
- 632 (31) Pochorovski, I.; Breiten, B.; Schweizer, W. B.; Diederich, F.  
633 FRET Studies on a Series of BODIPY-Dye-Labeled Switchable  
634 Resorcin[4]arene Cavitands. *Chem. - Eur. J.* **2010**, *16*, 12590–12602.
- 635 (32) Pagliusi, P.; Lagugn -Labarthe, F.; Shenoy, D. K.; Dalcanale, E.;  
636 Shen, Y. R. Sensing Vase-to-Kite Switching of Cavitands by Sum-  
637 Frequency Vibrational Spectroscopy. *J. Am. Chem. Soc.* **2006**, *128*,  
638 12610–12611.
- 639 (33) Gottschalk, T.; Jaun, B.; Diederich, F. Container Molecules with  
640 Portals: Reversibly Switchable Cycloalkane Complexation. *Angew.*  
641 *Chem., Int. Ed.* **2007**, *46*, 260–264.
- 642 (34) Busseron, E.; Rebek, J., Jr. Guest Recognition in a Partially  
643 Bridged Deep Cavitand. *Org. Lett.* **2010**, *12*, 4828–4831.
- 644 (35) Halgren, T. A. Merck molecular force field. II. MMFF94 van der  
645 Waals and electrostatic parameters for intermolecular interactions. *J.*  
646 *Comput. Chem.* **1996**, *17*, 520–552.
- 647 (36) Bianchi, F.; Mattarozzi, M.; Betti, P.; Bisceglie, F.; Careri, M.;  
648 Mangia, A.; Sidisky, L.; Ongarato, S.; Dalcanale, E. Innovative  
649 Cavitand-Based Sol–Gel Coatings for the Environmental Monitoring  
650 of Benzene and Chlorobenzenes via Solid-Phase Microextraction. *Anal.*  
651 *Chem.* **2008**, *80*, 6423–6430.
- 652 (37) Zhang, Z.; Zhu, L.; Ma, Y.; Huang, Y.; Li, G. Preparation of  
653 polypyrrole composite solid-phase microextraction fiber coatings by  
654 sol–gel technique for the trace analysis of polar biological volatile  
655 organic compounds. *Analyst* **2013**, *138*, 1156–1166.
- 656 (38) Silva, L. I. B.; Rocha-Santos, T. A. P.; Duarte, A. C. Remote  
657 optical fibre microsensor for monitoring BTEX in confined industrial  
658 atmospheres. *Talanta* **2009**, *78*, 548–552.